Physics-Guided Recurrent Graph Model for Predicting Flow and Temperature in River Networks

Xiaowei Jia[1], Jacob Zwart[2], Jeffrey Sadler[2], Alison Appling[2], Samantha Oliver[2], Steven Markstrom[2], Jared Willard[3], Shaoming Xu[3], Michael Steinbach[3], Jordan Read[2], and Vipin Kumar[3]

[1] University of Pittsburgh
[2] U.S. Geological Survey
[3] University of Minnesota

[1] xiaowei@pitt.edu, [2]{jzwart,jsadler,aappling,soliver,markstro,jread}@usgs.gov, [3]{willa099,xu000114,stei0062,kumar001}@umn.edu

Abstract—This paper proposes a physics-guided machine learning approach that combines advanced machine learning models and physics-based models to improve the prediction of water flow and temperature in river networks. We first build a recurrent graph network model to capture the interactions among multiple segments in the river network. Then we present a pre-training technique which transfers knowledge from physics-based models to initialize the machine learning model and learn the physics of streamflow and thermodynamics. We also propose a new loss function that balances the performance over different river segments. We demonstrate the effectiveness of the proposed method in predicting temperature and streamflow in a subset of the Delaware River Basin. In particular, we show that the proposed method brings a 33%/14% improvement over the state-of-the-art physics-based model and 24%/14% over traditional machine learning models (e.g., Long-Short Term Memory Neural Network) in temperature/streamflow prediction using very sparse (0.1%) observation data for training. The proposed method has also been shown to produce better performance when generalized to different seasons or river segments with different streamflow ranges.

I. INTRODUCTION

Machine learning (ML) models, which have found immense success in commercial applications, e.g., computer vision and natural language processing, are beginning to play an important role in advancing scientific discovery [1]–[3]. Given their power in automatically learning from observation data, ML models are particularly promising in scientific problems involving complex processes that are not completely understood by our current body of knowledge. However, scientific problems often involve non-stationary relationships among physical variables which can change over space and time. In the absence of adequate information about the physical mechanisms of real-world processes, traditional ML approaches are prone to false discoveries because it is difficult to capture these complex relationships solely from data. Moreover, the data available for many scientific problems is far smaller than what is needed to effectively train advanced ML models.

The focus of this paper is on modeling physical systems that have multiple interacting processes. In particular, we consider the application of predicting flow and temperature in river networks for both observed and unobserved river segments. In this problem, segments in the river network can show different flow and thermodynamic patterns driven by differences in catchment characteristics (e.g. slope, soil characteristics) and meteorological drivers (e.g. temperature, precipitation). These segments also interact with each other through the water advected from upstream to downstream segments. Moreover, there are often only a handful of river segments in a network that are monitored; thus there is limited data to train ML models. Accurate prediction of streamflow and water temperature aids in decision making for resource managers, establishes relationships between ecological outcomes and streamflow or water temperature, and helps predict other biogeochemical or ecological processes. For example, drinking water reservoir operators in the Delaware River Basin need to supply safe drinking water to New York City while also maintaining sufficient streamflow and cool water temperatures in the river network downstream of the reservoirs [4]. Accurate prediction of streamflow and water temperature helps managers optimize when and how much water to release downstream to maintain the flow and temperature regimes.

In scientific domains, physics-based models are often used to study engineering and environmental systems. Even though these models are based on known physical laws that govern relationships between input and output variables, most physics-based models are necessarily approximations of reality due to incomplete knowledge of certain processes or omission of processes to maintain computational efficiency. In particular, existing physics-based approaches for predicting river networks simulate the internal distribution of target variables (e.g., streamflow and temperature) based on general physical relationships such as energy and mass conservation. However, the model predictions still rely on qualitative parameterizations (approximations) based on soil and surficial geologic classification along with topography, land cover and climate input. Hence, such models can only provide sub-optimal prediction performance. Furthermore, calibration of physics-based models for river networks is often extremely time intensive due to interactions among parameters within segments and across segments and also requires expert knowledge of the system and model to calibrate successfully. The limitations of physics-based models cut across discipline boundaries and are well known in the scientific community; e.g., see a series of debate papers in hydrology [5]–[7].

Intuitively, we can model each river segment independently

by an individual ML model such as a Recurrent Neural Network (RNN). However, this approach has two major limitations: 1) In a river network, there exist many different types of river segments with diverse catchment characteristics (e.g., slopes, elevation, etc.). Note that most of the segments are poorly observed or completely unobserved, which makes it impossible to build a purely data driven model for each segment separately. 2) The individual models may ignore the rich spatial and temporal contextual information, e.g., how the streamflows from upstream segments impact the water temperature in downstream segments in the next few days.

The first issue could be partly addressed by pre-training the ML model using simulation data produced by physics-based models, but such pre-trained ML models still need some observations for refinement [8], [9]. In particular, for unobserved river segments, the performance of pre-trained ML models can be no better than physics-based models that can have rather poor performance. Addressing the second issue will require the development of sophisticated ML architecture that can leverage latent information that is transferred across river segments.

In this paper, we propose a global model, Physics Guided Recurrent Graph Networks (PGRGrN), which is applied to all the river segments. The architecture of PGRGrN is based on Recurrent Neural Networks (RNN) and Graph Convolutional Neural Networks (GCN), which explicitly captures the spatial interactions among different river segments as well as their temporal dynamics. Modeling of the spatial and temporal context is critical for the global ML model as it enables learning of different behavior patterns for different river segments even when they have similar input features on certain dates.

Design of such an architecture for this application faces two challenges. First, existing GCN-based models extract abstract latent variables (i.e., graph embeddings) to propagate over the networks but do not explicitly incorporate the prior physical knowledge about the interactions among different nodes. Such latent variables can become less informative when they are learned from sparser and less representative observation data, which can make the GCN model not generalizable. To address this challenge, we propose to utilize the intermediate variables simulated by the physics-based model to guide the learning process of the graph neural networks. This approach aims to enforce a physical interpretation to latent variables learned from each river segment by transferring the prior knowledge encoded by the physics-based model to the proposed ML model. Our experimental evaluation shows that this strategy is effective in initializing the ML model, which can then be fine-tuned using observations from the river network.

The second challenge is that target variables can vary drastically across different processes of a complex system. For example, streamflow can vary by several orders of magnitude across segments in a river network. When we train a global ML model over the entire river network, the training process using traditional loss functions (e.g., mean squared loss) tends to optimize the overall performance over training data available for the entire river networks, and thus can be dominated by river segments that contribute most to the overall error (e.g., segments with high streamflow). However, it is also important to accurately predict river segments with lower streamflow, as accurate prediction for these segments provides important information regarding the habitat for aquatic life and aquatic biogeochemical cycling. To address this challenge, we design a new loss function to ensure that the global ML model can simultaneously capture the local patterns of all the different segments. The local patterns of each segment can be extracted using an individual ML model trained only for this segment using simulation data (which is plentiful). Then during the training of the global ML model, we use a distance-based loss function, the contrastive loss function, to enforce its consistency with the extracted local patterns.

We implement our proposed method in a real-world dataset collected over 36 years from the Delaware River Basin located in the Northeast United States and demonstrate our method's superior predictive performance over existing methods. Moreover, we show that the proposed method produces much better prediction performance using sparse observations and also has better generalizability.

Our contributions can be summarized as follows:
- We introduce a new recurrent graph network architecture to model a river network with interacting river segments.
- We leverage knowledge from physics-based models to guide ML models for extracting latent variables, which helps initialize the model while enforcing consistency with known physical relationships amongst different processes.
- We propose a new contrastive loss function that balances the prediction performance over different river segments.
- We evaluate the utility in the context of an ecologically and societally relevant problem of monitoring river networks.

II. RELATED WORK

Recent works have shown the promise of integrating physics into ML models in improving the predictive performance and generalizability in scientific problems. This is commonly conducted in several ways, including developing new model architectures [10], [11], applying additional loss functions [8], [9], and modeling prediction residuals [12], [13]. When applied to systems with interacting processes, ML models are expected to have sufficient capacity to model such interactions. New ML architectures have been designed to enforce known physical relationships among multiple internal processes that jointly convert inputs to outputs [10], [11], [14], thus reducing the space for searching parameters. ML models have also shown great potential in modeling river networks [15], [16]. For example, Moshe et al. [16] propose HydroNets, which combines the information from each river segment and its upstream segments for improving streamflow predictions. It also learns local patterns for each basin by introducing basin-specific model layers in addition to the global model. This method focuses on predicting basins that are well monitored and it remains limited in generalizing to different scenarios

or learning with less data. In contrast, we leverage the prior physical knowledge to learn latent variables that make the model more generalizable.

The Graph Convolutional Networks (GCN) model has proven to be effective in automatically extracting latent factors that influence the neighbors in a graph. The use of GCN has also shown improved prediction accuracy in several scientific problems [17]–[19]. However, the information propagated amongst nodes in GCN is essentially an abstract representation learned by end-to-end training. Such abstract representations are not meant to enforce consistency with known physical relationships among different processes, such as in river networks.

Simulation data have been used to assist in training ML models. Since many ML models require an initial choice of model parameters before training, researchers have explored different ways to physically inform a model starting state. Poor initialization can cause models to anchor in local minima, which is especially true for deep neural networks. One way to harness physics-based modeling knowledge is to use the physics-based model's simulated data to pre-train the ML model, which also alleviates data paucity issues. Jia *et al.* extensively discuss this strategy [8]. They pre-train their Physics-Guided Recurrent Neural Network (PGRNN) models for lake temperature modeling on simulated data generated from a physics-based model and fine-tune it with little observed data. They show that pre-training can significantly reduce the training data needed for a quality model. In addition, Read et al. [20] show that such models are able to generalize better to unseen scenarios than pure physics-based models.

III. PROBLEM DEFINITION AND PRELIMINARIES

A. Problem definition

Our objective is to model the dynamics of temperature and streamflow in a set of connected river segments that together form a river network. The connections amongst these river segments can be represented in a graph structure $\mathcal{G} = \{\mathcal{V}, \mathcal{E}, \mathbf{A}\}$, where $\mathcal{V}$ represents the set of river segments and $\mathcal{E}$ represents the set of connections amongst river segments. Specifically, we create an edge $(i, j) \in \mathcal{E}$ if the segment i is anywhere upstream of the segment j. The matrix $\mathbf{A}$ represents the adjacency level between each pair of segments, i.e., $\mathbf{A}_{ij} = 0$ means there is no edge from the segment i to the segment j and a higher value of $\mathbf{A}_{ij}$ indicates that the segment i is closer to the segment j in terms of the river distance. More details of how we generate the adjacency matrix are discussed in Section V-A.

For each river segment i, we have access to its input features at multiple time steps $\mathbf{X}_i = \{\mathbf{x}_i^1, \mathbf{x}_i^2, ..., \mathbf{x}_i^T\}$. The input features $\mathbf{x}_i^t$ are a D-dimensional vector, which include meteorological drivers, geometric parameters of the segments, etc. (more details can be found in Section V-A). We also have a set of observed target variables $\mathbf{Y} = \{y_i^t\}$ but they are only available for certain time steps $t \in \{1, ..., T\}$ and certain segments $i \in \{1, ..., N\}$.

B. Physics-based Streamflow and Temperature Model

The Precipitation-Runoff Modeling System (PRMS) [21] and the coupled Stream Network Temperature Model (SNTemp) [22] is a physics-based model that simulates daily streamflow and water temperature for river networks, and other variables. PRMS is a one-dimensional, distributed-parameter modeling system that translates spatially-explicit meteorological information into water information including evaporation, transpiration, runoff, infiltration, groundwater flow, and streamflow. PRMS has been used to simulate catchment hydrologic variables at regional [23] to national scales [24] in support of resource management decisions, among other applications. The SNTemp module for PRMS simulates mean daily stream water temperature for each river segment by solving an energy mass balance model which accounts for the effect of inflows (upstream, groundwater, surface runoff), outflows, and surface heating and cooling on heat transfer in each stream segment. The SNTemp module is driven by the same meteorological drivers used in PRMS and also driven by the hydrologic information simulated by PRMS (e.g. streamflow, groundwater flow). Calibration of PRMS-SNTemp is extremely time-consuming because it involves a large number of parameters (84 parameters) and the parameters interact with each other both within segments and across segments.

C. Recurrent Neural Networks and Long-Short Term Memory

The RNN model has been widely used to model the temporal patterns in sequential data. The RNN model defines transition relationships for the extracted hidden representation through a recurrent cell structure. In this work, we adopt the Long-Short Term Memory (LSTM) cell which has proven to be effective in capturing long-term dependencies. The LSTM cell combines the input features $\mathbf{x}^t$ at each time step and the inherited information from previous time steps. Here we omit the subscript i as we do not target a specific river segment.

Each LSTM cell has a cell state $\mathbf{c}^t$, which serves as a memory and allows preserving information from the past. Specifically, the LSTM first generates a candidate cell state $\bar{\mathbf{c}}^t$ by combining $\mathbf{x}^t$ and the hidden representation at previous time step $\mathbf{h}^{t-1}$, as follows:

$$\bar{\mathbf{c}}^t = \tanh(\mathbf{W}_c^h \mathbf{h}^{t-1} + \mathbf{W}_c^x \mathbf{x}^t + \mathbf{b}_c). \tag{1}$$

Then the LSTM generates a forget gate f^t, an input gate g^t, and an output gate via sigmoid function $\sigma(\cdot)$, as follows:

$$\begin{aligned} \mathbf{f}^t &= \sigma(\mathbf{W}_f^h \mathbf{h}^{t-1} + \mathbf{W}_f^x \mathbf{x}^t + \mathbf{b}_f), \\ \mathbf{g}^t &= \sigma(\mathbf{W}_g^h \mathbf{h}^{t-1} + \mathbf{W}_g^x \mathbf{x}^t + \mathbf{b}_g), \\ \mathbf{o}^t &= \sigma(\mathbf{W}_o^h \mathbf{h}^{t-1} + \mathbf{W}_o^x \mathbf{x}^t + \mathbf{b}_o). \end{aligned} \tag{2}$$

The forget gate is used to filter the information inherited from $\mathbf{c}^{t-1}$, and the input gate is used to filter the candidate cell state at t. Then we compute the new cell state and the hidden representation as follows:

$$\begin{aligned} \mathbf{c}^t &= \mathbf{f}^t \otimes \mathbf{c}^{t-1} + \mathbf{g}^t \otimes \bar{\mathbf{c}}^t, \\ \mathbf{h}^t &= \mathbf{o}^t \otimes \tanh(\mathbf{c}^t), \end{aligned} \tag{3}$$

where $\otimes$ denotes the entry-wise product.

According to the above equations, we can observe that the computation of $\mathbf{h}^t$ combines the information at current time step ($\mathbf{x}^t$) and previous time step ($\mathbf{h}^{t-1}$ and $\mathbf{c}^{t-1}$), and thus encodes the temporal patterns learned from data.

IV. METHOD

In this section, we describe the details of the PGRGrN method. We start with introducing the model architecture. Then we discuss a strategy to help enforce physical relationships by leveraging the physical knowledge embedded in physics-based models. Finally, we introduce a contrastive loss function that attempts to ensure that the model performance on individual river segments is not compromised while optimizing the performance on the entire set of segments.
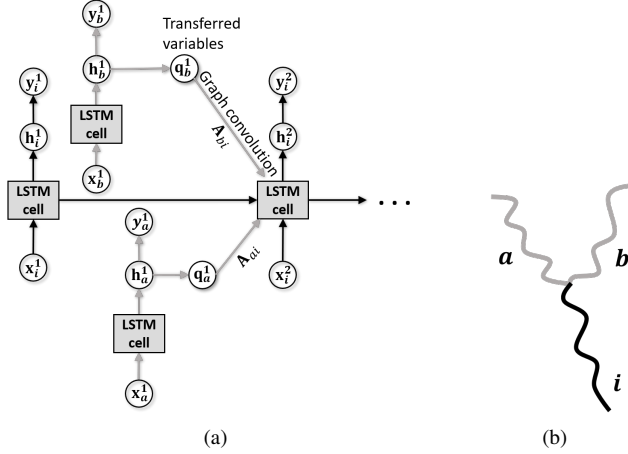

Fig. 1. (a) The RGrN architecture for an example river network with three segments (b). The segment a and the segment b are upstream of the segment i. The grey arrows indicate the modeling components for upstream segments.

A. Recurrent Graph Network

In a river network, most river segments are poorly observed or completely unobserved. To this end, we introduce a global ML model architecture, Recurrent Graph Network (RGrN), which is trained using data collected from all the river segments. Effective modeling of river segments requires the ability to capture their temporal dynamics and the influence received from upstream segments. Hence, we incorporate the information from both previous time steps and neighbors (i.e., upstream segments) when modeling each segment (Fig. 1).

Here we describe the recurrent process of generating the hidden representation $\mathbf{h}^t$ from $\mathbf{h}^{t-1}$, and we repeat this process for the entire sequence from $t = 2$ to T ($\mathbf{h}^1$ learned from an LSTM model). For each river segment i at time $t-1$, the model extracts latent variables which contain relevant information to pass to its downstream segments. We refer to these latent variables as transferred variables. For example, the amount of water advected from this segment and its water temperature can directly impact the change of water temperature for its downstream segments. We generate the transferred variables $\mathbf{q}_i^{t-1}$ from the hidden representation $\mathbf{h}_i^{t-1}$, as follows:

$$\mathbf{q}_i^{t-1} = \tanh(\mathbf{W}_q \mathbf{h}_i^{t-1} + \mathbf{b}_q), \tag{4}$$

where $\mathbf{W}_q$ and $\mathbf{b}_q$ are model parameters that are used to convert the hidden representation to transferred variables.

After gathering the transferred variables for all the segments, we develop a new recurrent cell structure for each segment i that integrates the transferred variables from its upstream segments into the computation of the cell state $\mathbf{c}_i^t$. This can be expressed as follows:

$$\mathbf{c}_i^t = \mathbf{f}_i^t \otimes (\mathbf{c}_i^{t-1} + \sum_{(j,i) \in \mathcal{E}} \mathbf{A}_{ji} \mathbf{q}_j^{t-1}) + \mathbf{g}_i^t \otimes \bar{\mathbf{c}}_i^t \tag{5}$$

We can observe that the forget gate not only filters the previous information from the segment i itself but also from its neighbors (i.e., upstream segments). Each upstream segment j is weighted by the adjacency level $\mathbf{A}_{ji}$ between j and i. When a river segment has no upstream segments (i.e., head water), the computation of $\mathbf{c}_i^t$ is the same as with the standard LSTM. In Eq. 5, we use $\mathbf{q}_j^{t-1}$ from the previous time step because of the time delay in transferring the influence from upstream to downstream segments (the maximum travel time is approximately one day according to PRMS). We also discuss the impact of increasing the time delay in Section V-G.

After obtaining the cell state, we can compute the hidden representation $\mathbf{h}_i^t$ by following Eq. 3. Finally, we generate the predicted output from the hidden representation as follows:

$$\hat{\mathbf{y}}_i^t = \mathbf{W}_y \mathbf{h}_i^t + \mathbf{b}_y, \tag{6}$$

where $\mathbf{W}_y$ and $\mathbf{b}_y$ are model parameters.

After applying this recurrent process to all the time steps, we define a loss using true observations $\mathbf{Y} = \{\mathbf{y}_i^t\}$ that are available at certain time steps and certain segments, as follows:

$$\mathcal{L}_{\text{RGrN}} = \frac{1}{|\mathbf{Y}|} \sum_{\{(i,t)|\mathbf{y}_i^t \in \mathbf{Y}\}} (\mathbf{y}_i^t - \hat{\mathbf{y}}_i^t)^2. \tag{7}$$

B. Transferring knowledge from physics-based models

The RGrN architecture has the capacity to model the latent information that is transferred across river segments. However, training RGrN directly in an end-to-end fashion can only learn an abstract representation for transferred variables while ignoring their physical interpretation. The transferred variables can become less informative when they are learned from sparser and less representative observation data. To this end, we introduce a new strategy to enforce the prior physical relationships amongst different river segments which are encoded by physics-based models. It helps make RGrN model more generalizable and also reduces the amount of observation data required to train a high-quality model. This strategy can be applied to a wide range of scientific problems that are modeled as a set of interacting processes.

We use the river temperature modeling as an example in this section to better illustrate the proposed strategy. For each river segment in the network, the temperature change is driven by energy exchanges caused by solar radiation, rainfall, evaporation, conductive and convective heat transfer, and net heat advected into river segments (e.g., groundwater flow, upstream flow, downstream flow). These energy fluxes

can be summarized into three categories and the process of temperature change conforms to the equation as follows:

$$\Delta \text{Temperature} \propto F_{in} - F_{out} + F_{up}, \qquad (8)$$

where F_{in} denotes the incoming energy fluxes from solar radiation, rainfall and other natural sources, F_{out} denotes the outgoing energy fluxes including long-wave emission, evaporation, conductive and convective heat transfer, and F_{up} denotes the net heat advected into the river segment from upstream segments. The term F_{up} can be estimated by a set of intermediate physical variables from upstream segments, which include upstream flow, upstream water temperature, relative humidity, and other physical characteristics. These intermediate physical variables can be simulated by PRMS-SNTemp internally.

Our goal is to ensure that the transferred variables $\mathbf{q}_i^t$ at each segment contain sufficient information to represent these intermediate physical variables so that downstream segments can gather all the information needed for capturing F_{up}. For each segment i at time t, we first simulate the set of intermediate variables $\mathbf{s}_i^t$ by running PRMS-SNTemp. Then we use $\mathbf{s}_i^t$ to add supervision on the transferred variables $\mathbf{q}_i^t$ such that we can extract $\mathbf{s}_i^t$ from $\mathbf{q}_i^t$. More formally, we define a loss function on transferred variables as follows:

$$\mathcal{L}_{\text{trans}} = \frac{1}{NT} \sum_i \sum_t ||\mathbf{s}_i^t - (\mathbf{W}_s \mathbf{q}_i^t + \mathbf{b}_s)||^2, \qquad (9)$$

where $\mathbf{W}_s$ and $\mathbf{b}_s$ are model parameters that convert transferred variables to the intermediate physical variables. We call this model as Physics-Guided Recurrent Graph Networks (PGRGrN) because we leverage the physical relationships between different river segments.

Since the computation of loss $\mathcal{L}_{\text{trans}}$ does not require observation data, we can use it to pre-train RGrN to enforce physical relationships. This pre-training method not only explicitly enforces the physical relationships among river segments, but also enables full usage of physical intermediates obtained from physics-based models to enhance the representation learned for $\mathbf{q}_i^t$ and its previous layer $\mathbf{h}_i^t$. In particular, the intermediate physical variables used in this work include streamflow, stream temperature, relative humidity, cloud cover, groundwater and shallow subsurface flow, and surface runoff.

It is noteworthy that the model extracts the intermediate variables from transferred variables $\mathbf{q}_i^t$ rather than forcing the transferred variables to be exactly the intermediate physical variables. Also, we optimize the loss $\mathcal{L}_{\text{trans}}$ in pre-training rather than using it as a regularizer in supervised learning. In other words, the ML model is guided but not constrained by the physics-based model output, which allows for more flexibility to automatically learn information in $\mathbf{q}_i^t$ that is poorly known or not yet discovered while also remaining helpful for modeling the interactions among river segments.

At the same time, we can run PRMS-SNTemp to simulate the final target variables corresponding to $\mathbf{y}_i^t$. Here we use $\tilde{\mathbf{y}}_i^t$ to represent the simulated target variables by PRMS-SNTemp. Although the simulated data are not accurate reflection of
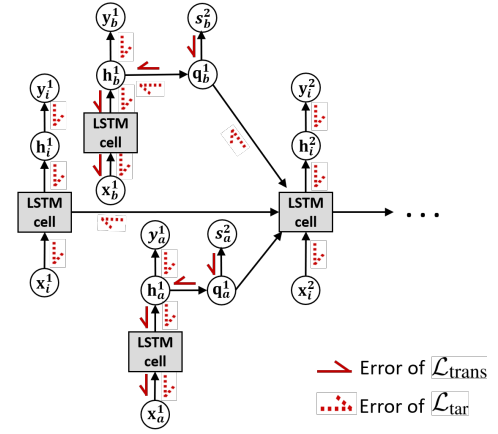

Fig. 2. Error back-propagation during pre-training stage.

the observation data, we can generate adequate simulations on every day and for every segment. The simulation data also follow many general physical relationships used to build the physics-based model. Given that observation data is often scarce, we can use simulated target variables to initialize the model via pre-training. Hence, we define another pre-training loss on target variables as follows:

$$\mathcal{L}_{\text{tar}} = \frac{1}{NT} \sum_i \sum_t (\tilde{\mathbf{y}}_i^t - \hat{\mathbf{y}}_i^t)^2, \qquad (10)$$

Combining Eqs. 9 and 10, we get the final pre-training loss as follows:

$$\mathcal{L}_{\text{pre}} = \mathcal{L}_{\text{tar}} + \lambda \mathcal{L}_{\text{trans}}, \qquad (11)$$

where λ is a hyper-parameter to balance two losses. The back-propagation of two losses is shown in Fig. 2.

In summary, our pre-training strategy helps initialize PGR-GrN using both simulated intermediate physical variables and simulated target variables. By enforcing known physical relationships between segments, the model becomes more generalizable. Besides, the ML model pre-trained with adequate simulated $\tilde{\mathbf{y}}$ can get much closer to its final optimal solution, and thus require fewer observation data for fine-tuning. We call this model which is pre-trained using simulation data and then fine-tuned with true observations as PGRGrN$^{\text{ptr}}$.

C. Segment-wise contrastive loss

The relationship between input features and target variables can be very complex in environmental systems, e.g., slight changes in segment slope and catchment size can drastically alter the streamflow. Traditional loss functions for regression problems, such as mean squared loss, tend to be dominated by river segments with larger errors while degrading the performance on other segments with smaller errors. This issue can be further exacerbated given limited observation data on most river segments, especially low-flow segments. Although improving the segments with smaller errors does not contribute much to reducing the overall error, accurately predicting streamflow at these segments provides important information regarding habitat for aquatic life and biogeochemical cycling.

We introduce a new loss function to balance the model performance over different segments, with the goal that the global ML model trained on all the river segments should also be consistent with the local patterns extracted from each river segment. In particular, we train N individual LSTM models, $\mathcal{M}_1$ to $\mathcal{M}_N$, for each segment using the simulation data. Each individual model $\mathcal{M}_i$ is trained to predict simulated target variables (i.e., $\tilde{\mathbf{y}}_i$) for a specific segment i. Even though there is a gap between simulation data and true observation data, these individual models have a better chance at capturing the local temporal patterns of each river segment.

When we apply the global PGRGrN model to a specific segment i, the patterns predicted by the PGRGrN model should be similar to the local patterns learned by the individual model $\mathcal{M}_i$. Specifically, we compute the hidden representation $\mathbf{h}_i^t$ from PGRGrN at each time t, which encodes dynamic patterns that directly output target variables. Similarly, we run the individual model $\mathcal{M}_i$ to compute its hidden representation $\tilde{\mathbf{h}}_i^t$, which encodes the local temporal patterns for this segment. The hidden representation $\mathbf{h}_i^t$ from PGRGrN should be close to the corresponding local hidden representation $\tilde{\mathbf{h}}_i^t$ and different from the local representation of other segments, i.e., $\tilde{\mathbf{h}}_j^t$ for $j \neq i$. More formally, define a contrastive loss as follows:

$$\mathcal{L}_{\text{ctr}} = -\frac{1}{NT}\sum_i\sum_t\log\frac{\exp(\mathbf{h}_i^{t\,T}\mathbf{W}_{ctr}\tilde{\mathbf{h}}_i^t)}{\sum_j\exp(\mathbf{h}_i^{t\,T}\mathbf{W}_{ctr}\tilde{\mathbf{h}}_j^t)}, \qquad (12)$$

where $\mathbf{W}_{ctr}$ is model parameters for computing the similarity of hidden representation. To ensure that the hidden representation produced by PGRGrN ($\mathbf{h}$) and by individual models ($\tilde{\mathbf{h}}$) are comparable, we use shared parameters $\{\mathbf{W}_y, \mathbf{b}_y\}$ in the last layer (Eq. 6) for individual models and the global PGRGrN model and they are fitted when training individual models.

By combining the contrastive loss and the loss of RGrN (Eq. 7), we get the fine-tuning loss as follows:

$$\mathcal{L}_{\text{finetune}} = \mathcal{L}_{\text{RGrN}} + \gamma\mathcal{L}_{\text{ctr}}, \qquad (13)$$

where γ is a hyper-parameter to balance the supervised loss of PGRGrN and the contrastive loss.

The proposed contrastive loss provides an alternative way in which different segments are comparable with each other. Traditional loss functions do not perform well for every segment because they are defined on target variables which may vary drastically across different segments. Instead, the contrastive loss matches temporal patterns encoded in the space of hidden representation, which alleviates this issue.

V. EXPERIMENTAL RESULTS

We evaluate the proposed method for predicting stream temperature and streamflow using real-world data collected from the Delaware River Basin, which is an ecologically diverse region and a societally important watershed along the east coast of the United States as it provides drinking water to over 15 million people [25]. We first describe our dataset and baselines. Then we discuss the results about the predictive performance using sparse data, the effectiveness

of pre-training, the spatial distribution of errors, and model generalization.

A. Dataset and baselines

The dataset is pulled from U.S. Geological Survey's National Water Information System [26] and the Water Quality Portal [27], the largest standardized water quality data set for inland and coastal waterbodies [27]. Observations at a specific latitude and longitude were matched to river segments that vary in length from 48 to 23,120 meters. The river segments were defined by the national geospatial fabric used for the National Hydrologic Model as described by Regan et al. [24], and the river segments are split up to have roughly a one day water travel time. We match observations to river segments by snapping observations to the nearest stream segment within a tolerance of 250 meters. Observations farther than 5,000 m along the river channel to the outlet of a segment were omitted from our dataset. Segments with multiple observation sites were aggregated to a single mean daily streamflow or water temperature value.

We study a subset of the Delaware River Basin with 42 river segments that feed into the mainstream Delaware River at Wilmington, DE. We use input features at the daily scale from Oct 01, 1980 to Sep 30, 2016 (13,149 dates). The input features have 10 dimensions which include daily average precipitation, daily average air temperature, date of the year, solar radiation, shade fraction, potential evapotranspiration and the geometric features of each segment (e.g., elevation, length, slope and width). Air temperature and precipitation values were derived from the Daymet gridded dataset. Other input features (e.g., shade fraction, solar radiation, potential evapotranspiration) are difficult to measure frequently, and we use values produced by the PRMS-SNTemp model as its internal variables. Water temperature observations were available for 32 segments but the temperature was observed only on certain dates. The number of temperature observations available for each segment ranges from 1 to 9,810 with a total of 51,103 observations across all dates and segments. Streamflow observations were available for 18 segments. The number of streamflow observations available for each segment ranges from 4,877 to 13,149 with a total of 206,920 observations across all dates and segments.

We generate the adjacency matrix $\mathbf{A}$ based on the river distance between each pair of river segment outlets, represented as $\text{dist}(i, j)$. We standardize the stream distance and then compute the affinity level as $\mathbf{A}_{ij} = 1/(1+\exp(\text{dist}(i, j)))$ for each edge $(i, j) \in \mathcal{E}$.

We compare model performance to multiple baselines, including the physics-based PRMS-SNTemp model, artificial neural networks (ANN), RNN with the LSTM cell, and the state-of-the-art PGRNN method [8] which uses simulation data to pre-train an LSTM model and then fine-tunes it with true observation data (represented as RNN$^{\text{ptr}}$). Since a region-specific calibration PRMS-SNTemp is extremely time-consuming, a version with default values of parameters is widely used in the hydrologic domain [28]. We provide a comparison with this

version referred to as the PRMS-SNTemp model. We evaluate three variants of the proposed method, RGrN (trained to minimize $\mathcal{L}_{\mathrm{RGrN}}$), PGRGrN$^{\mathrm{ptr}}$ (pre-training using the strategy in Section IV-B and fine-tuning to minimize $\mathcal{L}_{\mathrm{RGrN}}$, Eq. 7), and PGRGrN$^{\mathrm{ptr,ctr}}$ (pre-training using the strategy in Section IV-B and fine-tuning to minimize $\mathcal{L}_{\mathrm{finetune}}$, Eq. 13). All the ML models are trained and applied to all the river segments (i.e., all models are global). In the following experiments, we train each ML model using data from the first 24 years (Oct 01, 1980 to Sep 30, 2004) and then test in the next 12 years (Oct 01, 2004 to Sep 31, 2016). The hidden representation in these ML models is in 20 dimension (same for $\mathbf{q}_i^t$). We set the learning rate to be 0.0005 and update the model for 200 epochs for modeling water temperature and 300 epochs for modeling streamflow values.

B. Overall prediction performance

We report the testing performance of different methods for temperature prediction and streamflow prediction in Table I and Table II, respectively. We also test the capacity of each model to learn using less training data by randomly selecting 0.1% and 2% labeled data from first 24 years for training the model. For RNN$^{\mathrm{ptr}}$, PGRGrN$^{\mathrm{ptr}}$ and PGRGrN$^{\mathrm{ptr,ctr}}$, we assume the access to simulation data on every single date from Oct 01 1980 to Sep 20 2016 because they can be generated by simply running PRMS-SNTemp model on input drivers. We repeat each experiment five times with random model initialization and random selection of sparser data (0.1%, 2%) and report the mean and standard deviation of the root mean square error (RMSE).

We can observe that the proposed method outperforms baselines by a considerable margin (Tables I and II). The improvement from ANN to RNN shows that the recurrent component is helpful for capturing temporal patterns. RGrN performs better than RNN because it utilizes upstream-downstream dependencies which are critical for an accurate accounting of temperature and streamflow.

We also observe that PGRGrN$^{\mathrm{ptr}}$ has much better performance than RGrN using just 0.1% or 2% data. This is because we leverage the physical knowledge to add supervision on multiple model components (i.e., target variables and transferred variables) and thus the model can learn representative latent variables without risking overfitting small amount of observations. PGRGrN$^{\mathrm{ptr,ctr}}$ further improves the performance by adjusting the pre-trained model to conform to local patterns of each segment. The standard pre-training method is also helpful for the RNN model, as we can see the improvement from RNN to RNN$^{\mathrm{ptr}}$ using simulation data.

In Fig. 3, we show several examples for predictions made by PRMS-SNTemp (SIM), RNN, and the proposed model. In temperature prediction (Figs. 3 (a) and (b)), PRMS-SNTemp captures the overall dynamic patterns of temperature change but always has a bias to true observations. RNN gets closer to true observations but does not perform as well as PGRGrN$^{\mathrm{ptr,ctr}}$ in capturing fluctuations of temperature changes.

Method	0.1%	2%	100%
PRMS-SNTemp	3.661	3.661	3.661
ANN	3.706±0.114	2.159±0.059	1.575±0.035
RNN	3.234±0.057	1.908±0.048	1.546±0.045
RNN$^{\mathrm{ptr}}$	2.818±0.059	1.810±0.057	1.444±0.039
RGrN	2.849±0.049	1.906±0.063	1.408±0.068
PGRGrN$^{\mathrm{ptr}}$	2.556±0.045	1.715±0.041	1.406±0.035
PGRGrN$^{\mathrm{ptr,ctr}}$	2.464±0.105	1.636±0.056	1.402±0.034

Method	0.1%	2%	100%
PRMS-SNTemp	6.834	6.834	6.834
ANN	7.116±0.120	5.777±0.063	4.801±0.055
RNN	6.885±0.068	5.718±0.114	4.406±0.064
RNN$^{\mathrm{ptr}}$	6.367±0.067	5.529±0.053	4.104±0.049
RGrN	6.299±0.053	5.473±0.064	4.139±0.067
PGRGrN$^{\mathrm{ptr}}$	5.824±0.075	4.708±0.032	4.106±0.046
PGRGrN$^{\mathrm{ptr,ctr}}$	5.895±0.069	4.679±0.082	4.076±0.059

We can see similar results for predicting streamflow in segments with high flows (Fig. 3 (c)). Here PRMS-SNTemp produces a large bias and also a slow response. PGRGrN$^{\mathrm{ptr,ctr}}$ performs much better than both PRMS-SNTemp and RNN. However, for segments with low streamflows (Fig. 3 (d)), PRMS-SNTemp better matches with observations than ML models. This is because ML models optimize the overall performance while low-flow stream segments (mostly headwaters) are a minority in the entire river networks and contribute less to the loss function. In Fig. 3 (d), we show the results produced by variants of our method to study how the use of contrastive loss and pre-training alter the predictions. We can observe that the predictions made by RGrN are almost constant over time while PGRGrN$^{\mathrm{ptr}}$ can better capture the dynamics by pre-training the model but has an even larger gap with true observations. By adopting the contrastive loss, PGRGrN$^{\mathrm{ptr,ctr}}$ effectively reduces the bias on this low-flow segment.

To better understand how the performance varies across different types of river segments, we show the streamflow prediction errors for four types of segments, low ($<0.5m^3/s$), medium low ($0.5\text{-}2m^3/s$), medium high ($2\text{-}5m^3/s$) and high ($>5m^3/s$) in Fig. 4. RGrN and PGRGrN$^{\mathrm{ptr}}$ generally perform better than other methods in medium-high and high-flow river segments but perform much worse in low-flow segments. In particular, we can see RGrN has much larger errors than RNN over low-flow river segments. This is because the neighboring river segments tend to have similar embeddings after graph convolution and thus the training of RGrN pays even less attention to low-flow segments given the fact that there are only a few low-flow segments in the river network. As shown
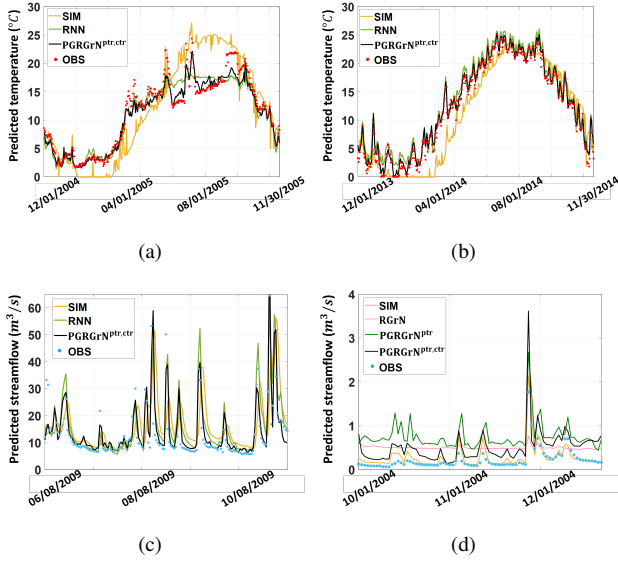
Fig. 3. (a)(b) Examples of temperature predictions by different methods. (c) An example of streamflow predictions in a high-flow river segment. (d) An example of streamflow predictions by variants of the proposed method in a low-flow river segment. Here SIM represents the simulated data produced by PRMS-SNTemp model and OBS represents the true observation data. Here we compare the performance of Recurrent Neural Networks (RNN), the proposed model Recurrent Graph Neural Networks (RGrN), the RGrN model using the pretraining strategy (PGRGrN^{ptr}) and the RGrN model using both pre-training and contrastive loss (PGRGrN^{ptr,ctr}).
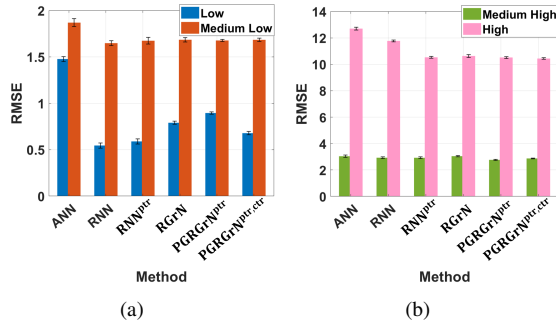

Fig. 4. Distribution of prediction errors in (a) low and medium-low segments, and (b) medium-high and high-flow segments.

in Fig. 4 (a), this issue is partly addressed by using the contrastive loss. An alternative solution to this issue is to intelligently select the most suitable model (e.g., PRMS-SNTemp or ML models) for different types of river segments, which we suggest as future work.

C. Assessing performance on unobserved segments

Here we aim to test the performance of models for the segments which have no observation data (Tables III and IV). Such segments commonly exist in a real-world basin system. Seg A to Seg E are five river segments which have sufficient observation data for both stream temperature and streamflow. Each row shows the results for an individual experiment where we intentionally remove the temperature or streamflow observations for a specific segment during the training period (Oct 01, 1980 to Sep 30, 2004). Then we report the prediction performance of RNN, RGrN, and PGRGrN^{ptr,ctr} only on this

Segment	Method	With Obs	Without Obs
Seg A	RNN	2.297±0.082	3.328±0.132
	RGrN	2.135±0.060	2.749±0.079
	PGRGrN^{ptr,ctr}	2.084±0.053	2.501±0.037
Seg B	RNN	1.116±0.064	1.384±0.065
	RGrN	0.981±0.037	1.214±0.032
	PGRGrN^{ptr,ctr}	1.047±0.024	1.205±0.016
Seg C	RNN	1.082±0.083	1.804±0.041
	RGrN	1.013±0.033	1.796±0.077
	PGRGrN^{ptr,ctr}	0.989±0.026	1.589±0.040
Seg D	RNN	0.955±0.053	1.805±0.064
	RGrN	0.902±0.026	1.597±0.024
	PGRGrN^{ptr,ctr}	0.996±0.025	1.297±0.017
Seg E	RNN	1.067±0.045	1.646±0.075
	RGrN	0.977±0.031	1.357±0.033
	PGRGrN^{ptr,ctr}	1.013±0.025	1.345±0.041

segment during the testing period (Oct 01, 2004 to Sep 31, 2016).

We can observe larger errors produced by all the three models after we remove training data for a segment. This is expected because segment-specific observation data has not been used for refinement of the model. However, we observe that the drop in performance of PGRGrN^{ptr,ctr} is consistent and often significantly smaller than that of the RNN model.

We notice that RGrN may not produce better streamflow predictions than RNN for every segment. For example, Seg A is a head water and has no upstream river segments. Hence, the graph convolution is not helpful for modeling Seg A. Besides, the information propagated from neighbors may not always be helpful if neighboring segments have very different streamflow patterns. A potential area of future research is to develop new graph operators so that each segment can only learn from neighbors that are most relevant.
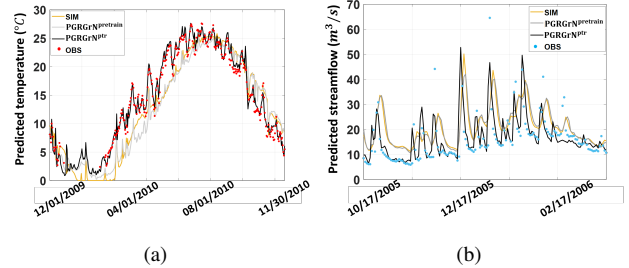

Fig. 5. The predictions of pre-trained (PGRGrN^{pretrain}) and fine-tuned models (PGRGrN^{ptr}) for (a) temperature and (b) streamflow, using 2% training data. Here we compare the performance of the RGrN model that is only pre-trained using simulation data (PGRGrN^{pretrain}) and the RGrN model using pre-training and then fine-tuned with observation data (PGRGrN^{ptr}).

D. Effectiveness of pre-training

In Fig. 5, we randomly select two example segments to show how predictions change from the pre-trained model (PGRGrN^{pretrain}) to the fine-tuned model (PGRGrN^{ptr}) using

TABLE IV

RMSE OF STREAMFLOW PREDICTION ON INDIVIDUAL SEGMENTS AFTER
REMOVING TRAINING OBSERVATION DATA. HERE WE COMPARE THE
PERFORMANCE OF RECURRENT NEURAL NETWORKS (RNN), THE
PROPOSED RECURRENT GRAPH NEURAL NETWORKS (RGrN) AND THE
RGrN MODEL USING BOTH PRE-TRAINING AND CONTRASTIVE LOSS
(PGRGrN$^{\text{PTR,CTR}}$).

Segment	Method	With Obs	Without Obs
Seg A	RNN	0.643±0.074	0.879±0.063
	RGrN	0.628±0.042	1.271±0.035
	PGRGrN$^{\text{ptr,ctr}}$	0.634±0.053	0.785±0.064
Seg B	RNN	3.231±0.054	3.493±0.112
	RGrN	3.185±0.066	3.234±0.045
	PGRGrN$^{\text{ptr,ctr}}$	2.981±0.067	3.043±0.091
Seg C	RNN	1.798±0.075	2.151±0.094
	RGrN	1.749±0.071	2.139±0.085
	PGRGrN$^{\text{ptr,ctr}}$	1.697±0.065	1.895±0.061
Seg D	RNN	1.983±0.103	2.711±0.114
	RGrN	2.006±0.110	2.354±0.077
	PGRGrN$^{\text{ptr,ctr}}$	1.989±0.084	2.343±0.079
Seg E	RNN	10.618±0.082	11.828±0.073
	RGrN	10.833±0.070	12.078±0.075
	PGRGrN$^{\text{ptr,ctr}}$	9.726±0.052	10.803±0.103

2% training data. Here the model PGRGrN$^{\text{ptr}}$ is the same with the PGRGrN$^{\text{ptr}}$ model used in the previous results but is only fine-tuned using 2% observations. In contrast, PGRGrN$^{\text{pretrain}}$ is only pre-trained using the strategy proposed in Section IV-B but without using observations for fine-tuning. Fig. 5 (a) shows that the pre-trained model match the simulated temperatures very well and thus can capture general temperature patterns even without using observation data. There is still a gap between true observations and PGRGrN$^{\text{pretrain}}$ since PGRGrN$^{\text{pretrain}}$ emulates PRMS-SNTemp, which has inherent bias due to an incomplete representation of physics. Nevertheless, after learning general patterns from simulation data, the model can be fine-tuned to match true observations using much less training data. This can be verified as we show that PGRGrN$^{\text{ptr}}$ fine-tuned with 2% data closes the gap between PGRGrN$^{\text{pretrain}}$ and true observations. Similarly, Fig. 5 (b) shows that pre-training helps capture general streamflow patterns and fine-tuning effectively fixes the bias and the slow response of PRMS-SNTemp.

E. Spatial distribution of errors

In Fig. 6, we show the distribution across different segments for ML temperature and streamflow prediction improvements over the physics-based PRMS-SNTemp simulations. In Fig. 6 (a), we can observe that RGrN and PGRGrN$^{\text{ptr,ctr}}$ produce smaller temperature error than RNN in many segments. We find one segment (in dashed circle) where RNN produces worse predictions than PRMS-SNTemp but RGrN greatly improves the prediction. This is the only segment in the data set for which we have no training data but sufficient testing data. The reason why RGrN can produce better predictions for this unlabeled segment is that it leverages the dependencies with other segments to learn the temperature patterns even without training data from this specific segment.

For streamflow prediction (Fig. 6 (b)), it can be seen that RGrN and PGRGrN$^{\text{ptr,ctr}}$ have lower RMSE in several high-

flow segments (e.g., the segments in red dashed circles). However, RGrN performs worse than RNN on headwater segments (in black dashed circles) and these segments have lower streamflow. Compared with RGrN, it can be seen that PGRGrN$^{\text{ptr,ctr}}$ alleviates this issue and produces smaller errors in these low-flow segments by using the contrastive loss.

F. Generalization test

Generalizability is important for scientific problems because most observation data can be collected from certain periods or locations for which it is easier to deploy sensors. Hence, we test model generazability for both streamflow and stream temperature prediction. In particular, we test the model performance on streamflow prediction using training data only from segments with higher average streamflows ($>3m^3/s$) in the first 24 years (Oct 1980 to Sep 2004). Then we report the RMSE in in the next 12 years for segments with lower average streamflows ($<1m^3/s$) in Table V. We also include the testing performance of the model trained using all the observations from first 24 years as a baseline in the second column of Table. V. Similarly, it is challenging for traditional ML models to generalize to predicting temperatures in a season that was not included in training data. We train each model using data only from colder seasons (spring, fall and winter) in the first 24 years and then test in summers in the next 12 years, as shown in Table VI.

Note that PGRGrN$^{\text{ptr,ctr}}$ always performs better than other methods because the incorporation of physical knowledge and minimizing the contrastive loss forces the model to learn generalizable patterns for each segment. It can be seen that ANN has large errors (especially in Table V) when applied to scenarios that are very different to training data. This is because ANN only focuses on the mapping from input features to target variables while physical phenomena are often driven by spatial and temporal processes. Such a gap makes ANN prone to overfit the training data. In contrast, RGrN performs better than ANN and RNN in temperature prediction because it leverages the dependencies both over space and time, and thus has a better chance in learning generalizable patterns. However, the performance of RGrN becomes worse in predicting segments with lower streamflows. The graph convolution makes the extracted hidden representation ($\mathbf{h}_i^t$) more similar for neighboring segments and thus RGrN simulate streamflows with similar dynamic patterns as in high-flow segments when it is trained just using observation data from high-flow segments.

G. Sensitivity tests

Here we test the sensitivity of the model to different hyperparameter settings. Also we test the performance of the model with different time delays (Eq. 5).

In Figs. 7 (a) and (b), we show the prediction performance using 2% data using different values of λ (Eq. 11) and γ (Eq. 13). We can see that the model is relatively robust with different values of hyper-parameters but there is a slight increase of RMSE if we set γ and λ to be either too small or too large. With a small γ, the model has less weight on
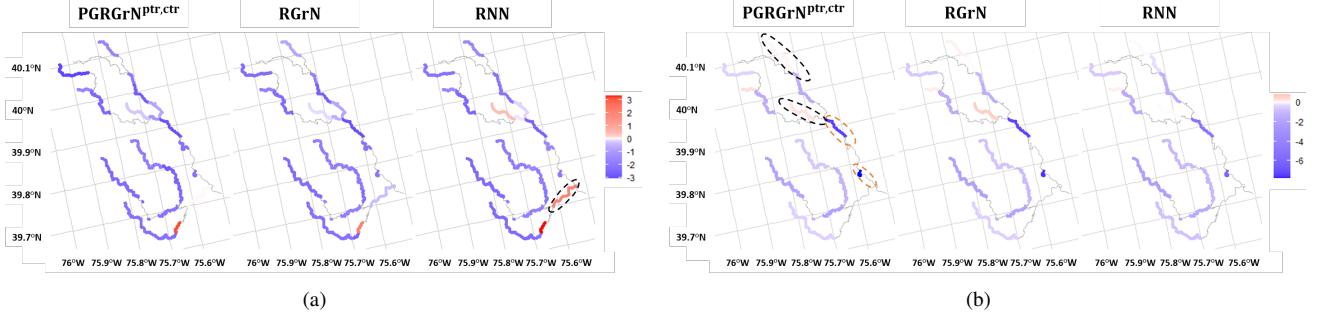
Fig. 6. Prediction errors across different segments for (a) temperature prediction and (b) streamflow prediction. Here we show the error as the RMSE of each method minus the RMSE of PRMS-SNTemp simulation data to get a better contrast. Darker blue indicates better performance of the ML model over the physics-based model. In (a), we do not discuss the red colored segment on the bottom (predicted poorly by all the three methods) and head water ($75.7°$W, $39.95°$N) predicted poorly by RNN because they just have one test observation.

Method	Train on high-flow	Train on all the data
ANN	9.752±0.527	1.719±0.114
RNN	3.012±0.432	1.196±0.054
RNN$^{\text{ptr}}$	3.279±0.526	1.075±0.063
RGrN	4.073±0.082	1.212±0.066
PGRGrN$^{\text{ptr}}$	2.226±0.089	1.206±0.076
PGRGrN$^{\text{ptr,ctr}}$	2.099±0.088	1.201±0.089

Method	Train on cold seasons	Train on all the data
ANN	2.138±0.093	1.794±0.032
RNN	2.104±0.080	1.789±0.034
RNN$^{\text{ptr}}$	1.893±0.085	1.555±0.021
RGrN	1.939±0.062	1.539±0.024
PGRGrN$^{\text{ptr}}$	1.853±0.034	1.530±0.014
PGRGrN$^{\text{ptr,ctr}}$	1.744±0.053	1.416±0.019

contrastive loss and thus produces worse performance using limited (2%) observation data. With a large γ value, we put a higher weight on the contrastive loss but the model is more likely to be impacted by the bias in the simulation data. On the other hand, the smaller value of λ will make the model ignorant of the supervision on transferred variables while a much larger value of λ results in less focus on the target variables. It is worth mentioning that our adopted hyperparameters may not be optimal values in the testing set because they are tuned using the simulation data.

In Figs. 7 (c) and (d), we use different lengths of time delay, from one time step to five time steps, in Eq. 5. The time delay

indicates how many days prior the information from upstream segments influence the downstream segments. We can see a general increase of RMSE when we set a larger time delay.
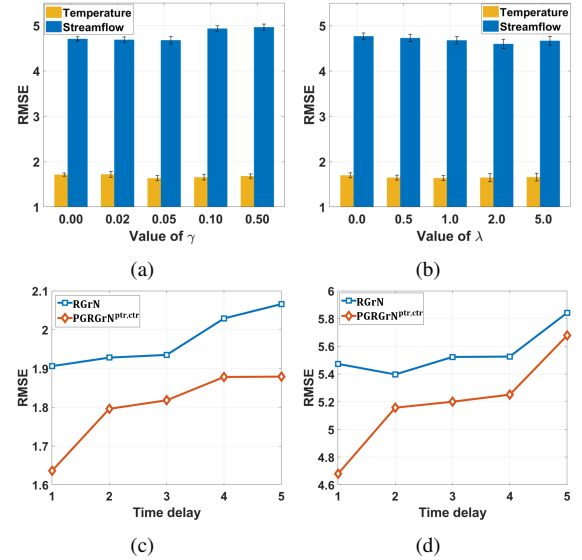

Fig. 7. Performance using different values of (a) γ and (b) λ. Performance with different time delay for (c) temperature and (d) streamflow prediction. In (c) and (d) we sohw the performance of the proposed Recurrent Graph Neural Networks (RGrN) and the RGrN model using both pre-training and contrastive loss (PGRGrN$^{\text{ptr,ctr}}$).

VI. CONCLUSION

In this paper, we propose a novel method PGRGrN for modeling interacting segments in river networks. We leverage the prior physical knowledge about segment-to-segment interactions embedded in physics-based models to enhance the learning of latent representation in the proposed ML model. Moreover, we improve the loss function to optimize both the overall performance over the river network and the local performance on each individual river segment. We have demonstrated the superiority of the proposed method in handling the scarcity of labeled data and in generalizing to unseen scenarios.

In addition to modeling variables in river networks, the proposed method can be adjusted to model other complex

systems which involve interacting processes. For example, this method could be potentially used for material discovery, biological research and quantum chemistry to capture interactions between different atoms or molecules.

While our method performs much better than existing models, it remains limited in precisely predicting special segments (e.g., unobserved segments and segments with extremely low streamflows). To advance understanding, future ML modeling efforts may consider uncertainty of the global ML model and determine whether ML should be used to replace physics-based models in different situations.

VII. ACKNOWLEDGMENTS

REFERENCES

[1] D. Graham-Rowe, D. Goldston, C. Doctorow, M. Waldrop, C. Lynch, F. Frankel, R. Reid, S. Nelson, D. Howe, S. Rhee *et al.*, "Big data: science in the petabyte era," *Nature*, vol. 455, no. 7209, pp. 8–9, 2008.

[2] T. Jonathan, A. Gerald, B. Sandrine *et al.*, "Special online collection: dealing with data," *Science*, vol. 331, no. 6018, pp. 639–806, 2011.

[3] T. J. Sejnowski *et al.*, "Putting big data to good use in neuroscience," *Nature neuroscience*, vol. 17, no. 11, p. 1440, 2014.

[4] A. Ravindranath, N. Devineni, and P. Kolesar, "An environmental perspective on the water management policies of the upper delaware river basin," *Water Policy*, vol. 18, no. 6, pp. 1399–1419, 2016.

[5] U. Lall, "Debates—the future of hydrological sciences: A (common) path forward? one water. one world. many climes. many souls," *Water Resources Research*, vol. 50, no. 6, pp. 5335–5341, 2014.

[6] H. V. Gupta and G. S. Nearing, "Debates—the future of hydrological sciences: A (common) path forward? using models and data to learn: A systems theoretic perspective on the future of hydrological science," *Water Resources Research*, 2014.

[7] J. J. McDonnell and K. Beven, "Debates—the future of hydrological sciences: A (common) path forward? a call to action aimed at understanding velocities, celerities and residence time distributions of the headwater hydrograph," *Water Resources Research*, vol. 50, no. 6, pp. 5342–5350, 2014.

[8] X. Jia, J. Willard, A. Karpatne, J. Read, J. Zwart, M. Steinbach, and V. Kumar, "Physics guided rnns for modeling dynamical systems: A case study in simulating lake temperature profiles," in *Proceedings of the 2019 SIAM International Conference on Data Mining*. SIAM, 2019, pp. 558–566.

[9] J. S. Read, X. Jia, J. Willard, A. P. Appling, J. A. Zwart, S. K. Oliver, A. Karpatne, G. J. Hansen, P. C. Hanson, W. Watkins *et al.*, "Process-guided deep learning predictions of lake water temperature," *Water Resources Research*, 2019.

[10] B. Anderson, T. S. Hy, and R. Kondor, "Cormorant: Covariant molecular neural networks," in *Advances in Neural Information Processing Systems*, 2019, pp. 14 510–14 519.

[11] N. Muralidhar, M. R. Islam, M. Marwah, A. Karpatne, and N. Ramakrishnan, "Incorporating prior domain knowledge into deep neural networks," in *2018 IEEE International Conference on Big Data (Big Data)*. IEEE, 2018, pp. 36–45.

[12] J.-X. Wang, J.-L. Wu, and H. Xiao, "Physics-informed machine learning approach for reconstructing reynolds stress modeling discrepancies based on dns data," *Physical Review Fluids*, 2017.

[13] D. Liu and Y. Wang, "Multi-fidelity physics-constrained neural network and its application in materials modeling," *Journal of Mechanical Design*, vol. 141, no. 12, 2019.

[14] J. Park and J. Park, "Physics-induced graph neural network: An application to wind-farm power estimation," *Energy*, 2019.

[15] F. Kratzert, D. Klotz, M. Herrnegger, A. K. Sampson, S. Hochreiter, and G. S. Nearing, "Toward improved predictions in ungauged basins: Exploiting the power of machine learning," *Water Resources Research*, 2019.

[16] Z. Moshe, A. F. Metzger, F. Kratzert, G. Elidan, S. Nevo, and R. El-Yaniv, "Hydronets: Leveraging river structure for hydrologic modeling," 2020.

[17] Y. Qi, Q. Li, H. Karimian, and D. Liu, "A hybrid model for spatiotemporal forecasting of pm2. 5 based on graph convolutional neural network and long short-term memory," *Science of the Total Environment*, 2019.

[18] T. Xie and J. C. Grossman, "Crystal graph convolutional neural networks for an accurate and interpretable prediction of material properties," *Physical review letters*, vol. 120, no. 14, p. 145301, 2018.

[19] D. Zhu *et al.*, "Understanding place characteristics in geographic contexts through graph convolutional neural networks," *Annals of the American Association of Geographers*, 2020.

[20] J. S. Read *et al.*, "Process-guided deep learning predictions of lake water temperature," *Water Resources Research*, 2019.

[21] S. L. Markstrom *et al.*, "Prms-iv, the precipitation-runoff modeling system, version 4," *USGS Techniques and Methods*, no. 6-B7, 2015.

[22] M. J. Sanders, S. L. Markstrom, R. S. Regan, and R. D. Atkinson, "Documentation of a daily mean stream temperature module—an enhancement to the precipitation-runoff modeling system," US Geological Survey, Tech. Rep., 2017.

[23] J. H. LaFontaine *et al.*, "Application of the precipitation-runoff modeling system (prms) in the apalachicola-chattahoochee-flint river basin in the southeastern united states," *USGS Scientific Investigations Report*, 2013.

[24] R. S. Regan, S. L. Markstrom, L. E. Hay, R. J. Viger, P. A. Norton, J. M. Driscoll, and J. H. LaFontaine, "Description of the national hydrologic model for use with the precipitation-runoff modeling system (prms)," US Geological Survey, Tech. Rep., 2018.

[25] T. N. Williamson, J. G. Lant, P. Claggett, E. A. Nystrom, P. C. Milly, H. L. Nelson, S. A. Hoffman, S. J. Colarullo, and J. M. Fischer, "Summary of hydrologic modeling for the delaware river basin using the water availability tool for environmental resources (water)," US Geological Survey, Tech. Rep., 2015.

[26] U. G. Survey, "National water information system data available on the world wide web (usgs water data for the nation)," 2016.

[27] E. K. Read *et al.*, "Water quality data for national-scale aquatic research: The water quality portal," *Water Resources Research*, 2017.

[28] R. S. Regan *et al.*, "Description of the national hydrologic model for use with the precipitation-runoff modeling system (prms)," US Geological Survey, Tech. Rep., 2018.